Journal of
Nanoscience and Nanotechnology
Vol. 7, 3421–3430, 2007

Decarboxylation of Oxidized Single-Wall Carbon Nanotubes

H. S. Vieira[1], D. M. Andrada[1], R. Mendonça[1], A. P. Santos[1], M. D. Martins[1], W. A. A. Macedo[1], H. F. Gorgulho[2], L. P. S. Pimenta[3], R. L. Moreira[3], A. Jorio[3], M. A. Pimenta[3], and C. A. Furtado[1,*]

[1] *Centro de Desenvolvimento da Tecnologia Nuclear – CDTN/CNEN – C. P. 941, 30123-970 – Belo Horizonte – MG, Brazil*
[2] *Universidade Federal de São João del-Rei – 36307-352 – São João del-Rei – MG, Brazil*
[3] *Universidade Federal de Minas Gerais – 31270-901 – Belo Horizonte – MG, Brazil*

A classical protocol widely used in organic chemistry of aromatic and polyaromatic molecules has been successfully applied in this work for the decarboxylation of oxidized single-wall carbon nanotube (SWNT) to rend C–H SWNT derivatives. SWNT produced by arc discharge method have been oxidized during a purification process using strongly oxidant agents, such as hydrogen peroxide and nitric acid. The decarboxylation of oxidized SWNT has been conduced with copper(I) oxide in a 50:50 solution of *N*-methylpyrrolidone and quinoline. Fourier transform infrared spectroscopy, X-ray photoelectron spectroscopy and acid-base potentiometric titration analyses were carried out to characterize quali and quantitatively the changes in the chemical environment on the SWNT surface in each step of the purification and the decarboxylation process. Those techniques showed the appearance of mainly carboxylic and phenolic groups after the purification process and the disappearance of the carboxylic groups after the decarboxylation reaction. Fourier transform infrared spectroscopy analysis indicated also the formation of aliphatic and aromatic C–H groups. X-ray photoelectron spectroscopy and potentiometric titration results determined an efficiency higher than 90% for our decarboxylation procedure. The purity and structural quality of the SWNT sample used in the decarboxylation process were evaluated by thermogravimetry and Raman spectroscopy. Thermogravimetric analysis identified a purified sample with ~80 wt% of SWNT, in fractions distributed in highly structured SWNTs (25 wt%), with distribution in composition, length and structural quality (35 wt%) and with very defective and short tubes (25 wt%). The damages on the purified SWNT walls were characterized by the Raman scattering analysis.

Keywords: Single-Wall Carbon Nanotubes, Functionalization, Characterization.

1. INTRODUCTION

A single-wall carbon nanotube (SWNT) corresponds to a graphene sheet rolled up as a cylinder, with diameter of about 1 nm. These nanostructures have been the focus of intensive fundamental studies over the last decade, due to their unique electronic and mechanical properties.[1,2] They have been considered for applications in molecular electronics, sensing, gas storage, field-emission devices, biological molecules and catalyst supports, and high strength fibers for the next generation of high-performance composites. However, an intimate understanding of the chemistry and functionality of carbon nanotubes is of major importance for the development of their science and applications. The ability to carry out controlled chemistry on the carbon nanotube surface and characterize the physico-chemical properties of the derivatives is important to obtain new molecules with chemical selectivity and will play an essential role in the realization of the promise of this material.

In terms of chemical reactivity, the carbon nanotube molecule could be divided into two parts:
(a) the sidewall, and
(b) the defect sites and end caps.[3]

In the first case, several chemical modification routes have been explored, but sometimes with the disadvantage of concomitant loss of the carbon nanotube conjugated electronic structure.[4] In the latter case, the intrinsic defects, such as pentagon–heptagon pairs, sp^3-hybridized carbon atoms, and vacancies in the nanotube lattice can be supplemented by additional damage and functionalization from

*Author to whom correspondence should be addressed.

strongly oxidative purification procedures. Many growth processes of large batches of bundled, free-standing SWNTs produce samples that are not pure and contain residual growth catalyst and amorphous carbon as important impurities.[5–9] The manufacturing and post-synthesis chemical purification are mostly based on acid or dry oxidation which can remove C-atoms from the tube wall, open the tubes and add functional groups such as carboxylic acid, ketone, alcohol, and ester to the SWNT surface.[10, 11] Subsequent chemical derivatization on these oxygenated functional groups has been explored to render the SWNT soluble, and attach SWNTs to nanoparticles, small, macro, and bio molecules.[4, 12]

In this work, we propose a new functionalization route for the open end caps of SWNT, where decarboxylation of oxidized SWNTs rends C–H SWNT derivatives. As reported by Khare et al.,[13] the introduction of C–H bonds in SWNTs is expected to alter transport properties that may lead to useful semiconducting devices and may impart radiation shielding properties to composites for space applications. Besides that, C–H SWNT derivatives could be a start molecule for new chemical reactions on the SWNT surface. Here, SWNTs produced by the arc discharge method have been oxidized during a purification process using strongly oxidant agents, such as hydrogen peroxide and nitric acid. The decarboxylation of oxidized SWNTs has been conducted with copper(I) oxide in a 50:50 solution of *N*-methylpyrrolidone and quinoline. This classical "Organic Chemistry" reaction, firstly proposed by Shepard, Winslow, and Johnson in 1930,[14] has been amply used for the decarboxilation of aromatic and polyaromatic carboxylic acids.[15, 16] We have optimized our procedure for the SWNT molecules from works of Cohen et al.[15, 16] The SWNT derivatives obtained in each step of the functionalization route have been characterized by thermogravimetry (TG), fourier transform infrared spectroscopy (FTIR), Raman scattering, X-ray photoelectron spectroscopy (XPS), and potenciometric titration. Since the relative amount of chemically reactive sites on the SWNT surface (ends and defects) is not large (<5 wt%) and the C–H SWNT derivative is not expected to be soluble, a careful and systematic characterization study was carried out. This work represents a fundamental study using spectroscopic and analytical techniques to observe the effect of model compound reactions on SWNT molecules in obtaining chemically selective SWNT derivatives.

2. EXPERIMENTAL DETAILS

Arc discharge nanotube soot was obtained from Carbolex, Inc. One "selected grade" batch from the vendor was homogenized and studied here. The tubes were produced using ~4 atomic% Ni–Y loaded carbon electrodes. The as-delivered material was found to contain bundles of SWNTs, with mean nanotube diameter ~1.5 nm, as determined by Raman spectroscopy. Also present in the soot is ~32 wt% amorphous carbon and ~33 wt% of carbon-coated Ni–Y particles, as determined by thermogravimetric analysis in air (Fig. 1).

A two step oxidative purification procedure was used to purify the as-grown SWNTs:
(1) wet oxidation removal of amorphous carbon was carried out by refluxing in 30 vol.% of H_2O_2 in H_2O (0.2 liter of solution per 1.0 g of raw material) for 2 h.

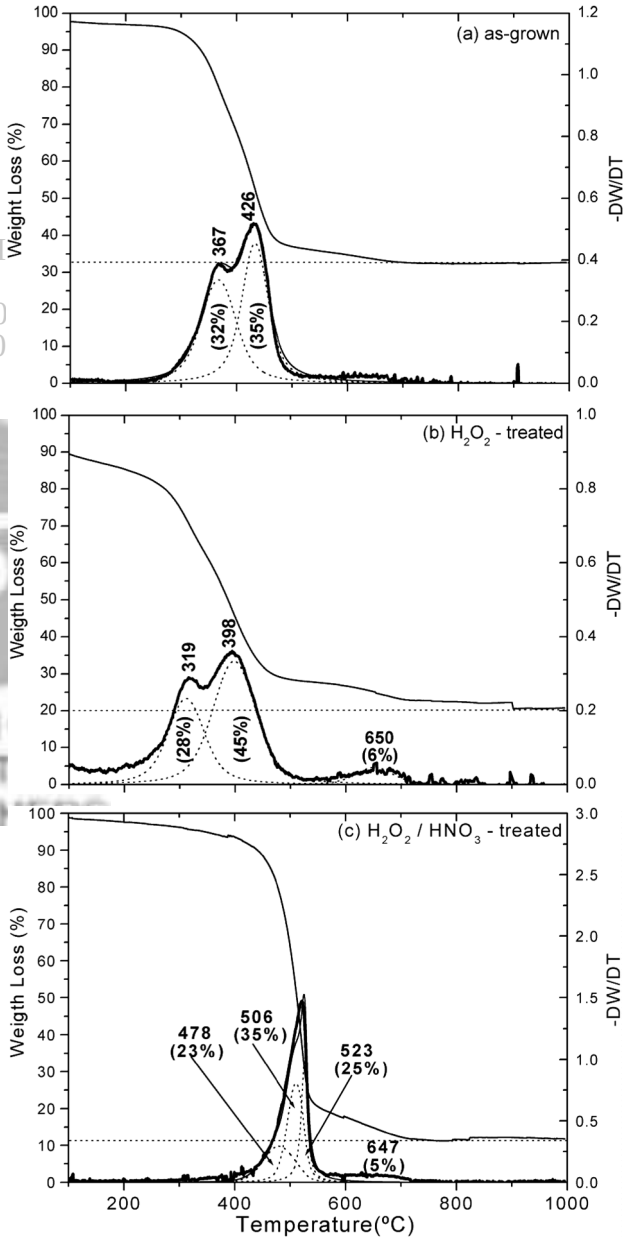

Fig. 1. TG curves of the as-grown SWNT (a) and chemically processed SWNT materials: H_2O_2-treated (b) and H_2O_2/HNO_3-treated (c). The solid, dash, and dot lines correspond to TG, DTG, and Lorentzian fit of DTG curves, respectively. The Lorentzian line shape analysis parameters (peak position and % area under curve) for the DTG curves are indicated in the figure.

The solution was then cooled to room temperature and filtered through a 1.0 μm pore-sized polycarbonate membrane (Whatman, Inc.);
(2) for metal removal (Ni–Y), we refluxed the material produced by step 1 in a strongly oxidizing 3N HNO_3 solution for 15 h.

The mixture was cooled to room temperature, diluted with distilled water, and filtered through a 0.45 μm pore-sized membrane. The filtrate on the membrane was exhaustively washed with NaOH solution and distilled water until pH neutral for solubilization of small oxidized and functionalized polycyclic aromatic sheets. The samples were then dried under vacuum at 120 °C for 12 h. The details of metal removal procedure can also be found in Ref. [8]. This procedure is known to lead to SWNT bundles with open ends and functionalized with mainly carboxylic acid groups.[10]

For the decarboxylation reaction, it was employed high-purity grade reagents and solvents and the quinoline was distilled before use. The purified SWNT material (~20 mg) was added to a three-neck round bottom flask containing a magnetic stirring bar fitted with a condenser, a thermometer, and a gas inlet tube, containing 10 ml of quinoline, 10 ml of *N*-methylpyrrolidinone and 34 mg of cuprous oxide. The mixture was maintained at 210 °C for 12 h under inert argon atmosphere. The mixture was then cooled to room temperature, diluted with methanol, and filtered through a 0.45 μm pore-sized membrane. The filtrate was suspended in 0.1 N HNO_3 solution to remove any copper and derivative precipitates. The mixture was diluted with distilled water, filtered again through a 0.45 μm pore-sized membrane and washed until pH neutral. The new filtrate was dried under vacuum at 120 °C for 12 h.

TG measurements were performed in a Simultaneous DTA-TGA—TA Instrument analyzer where samples of approximately 5 mg were heated from 25 to 1000 °C at a scan rate of 5 °C · min^{-1} in dry air atmosphere at 100 ml · min^{-1}.

Samples for Raman scattering studies were prepared by placing a few drops of SWNT/isopropanol suspension on a warm ~60 °C glass substrate. Micro-Raman spectra were collected using a Dilor XY triple-monochromator spectrometer equipped with a confocal microscope (Olympus BH-2) and a CCD detector. The scattering was excited using an argon ion laser (514.5 nm), and the power measured at the sample was 1 mW inside a 1 μm laser spot size. This particular excitation wavelength primarily couples to the semiconducting tubes in the sample.[17, 18]

Infrared spectra in the 750–4000 cm^{-1} wavenumber range were collected in the transmission mode of a Centaurus microscope (magnification 10X, observed region 150 × 150 μm^2) attached to a FTIR Nicolet (Nexus 470) spectrometer. The spectral resolution was better than 4 cm^{-1} and the spectra were averaged over 64 scans. The spectrometer configuration was: Ever-glow source, Ge-coated KBr beamsplitter, and HgCdTe detector, under nitrogen purge. For the FTIR measurements, the nanotube material was ultrasonicated in isopropanol for 15 minutes using a low power bath. This suspension was then centrifuged in an Eppendorf 5417C centrifuge for 2 minutes at 2000 g. Several drops of the supernatant liquid were then deposited onto non-doped silicon substrates (highly transparent in the infrared region) and maintained in air at ~60 °C via the drop/dry technique until a transparent bundled nanotube film was obtained. The reference spectra were taken in the same silicon sample, in regions with no organic trace.

X-ray photoelectron spectroscopy measurements were performed using a non-monochromatic Al Kα 1486.3 eV X-ray source and a VG CLAM II hemispherical electron-energy analyzer in a UHV system at a base pressure of 5×10^{-10} mbar. The carbon nanotubes were mounted in a KBr (Merck, for spectroscopy) pellet holder and the C1s high resolution spectra were taken with 20 eV pass-energy. The fits were done by a combination of Gaussian and Lorentzian curves and a Shirley-type background subtraction in SDP program.

Potentiometric titration was carried out with an automatic microburette system Titroline ALPHA from SCHOTT S.A. interfaced with a microcomputer. The SWNT samples (~5 mg) were added to an electrochemical cell with 1.0 ml HCl 0.103 mol $liter^{-1}$ under N_2 atmosphere, with ionic force adjusted to 0.10 mol $liter^{-1}$ with KCl to make up a total volume of 20 ml. The pH was monitored until equilibrium was reached, after which NaOH 0.0984 mol $liter^{-1}$ titration was started. Titration was carried out with 0.01-ml injections at 100-s intervals. Potentiometric titration curves were fit by a nonlinear method based on the general equation that describes the titration of the mixture of a strong acid with *n* acids (surface groups).[19]

3. RESULTS AND DISCUSSION

3.1. Thermogravimetric Analysis

The composition and purity of as-grown and chemically processed SWNT samples were evaluated using thermogravimetric analysis through the line shape analysis of DTG data by Lorentzian curves.[20, 21] Although the carbon nanotube community is quite used to take advantage of line shape analysis for spectroscopic data, it seems that there is a concern about applying this approach for thermogravimetric results, mainly because of the high overlapping of the decomposition steps and bad quality of the fittings.[21] As-grown and moderately purified samples are the most challenging systems for this study because of the presence of different carbonaceous fractions, the possibility of their co-decomposition and the oxidative catalytic effect of metal particles. However, by working along together with other techniques like Raman spectroscopy and XPS, as done in the present work, makes us confident in considering the contribution of this kind of

fitting procedure as a guide for a quantitative evaluation of the composition of the SWNT samples.

Figure 1 shows the TG curve and the Lorentzian line shape analysis of the DTG results of the SWNT samples: as-grown (a) and after the sequential steps of carbon nanotube purification (b) and (c). The TG curve of the as-grown sample exhibits two prominent weight losses of ~32 and 35% with corresponding sharp DTG peaks at 367 and 426 °C, initially due to the decomposition of preferentially amorphous carbon and SWNT, respectively.[5, 20, 21] The ~33 wt% of residual material refers to the oxidized metal (Ni–Y) catalyst particles. The H_2O_2 treatment (reflux for 2 h in a 30 vol.% solution) was not efficient in removing amorphous carbon, but it was enough to oxidize the carbonaceous material around the metal particles exposing them and helping their removal in the next purification step (HNO_3 treatment). The more exposed metal particles act as a localized heat source decreasing the burning temperature of the carbon forms present in the sample.[22] This explain the downshift of the DTG peaks to 319 and 398 °C in Figure 1(b). The broader peak related to the SWNT fraction is a reflex of the sample heterogeneity and the proximity or not to the metal particles.[21] After the two-step purification procedure (Fig. 1(c)), practically only one narrow and prominent weight loss of ~83% was observed and the residue amount decreased to 11 wt%. The metal remain is probably well encapsulated in amorphous-graphitic particles and the oxidation of these will be at the same time to the oxidation of metals. The main carbonaceous decomposition event between 450 and 550 °C was better fit with three Lorentzian lines. The DTG peak at ~523 °C corresponding to 25 wt% is due to the high-purity SWNT fraction (the SWNT are not in close contact with catalysts). The two other SWNT decompositions are probably assisted by metals.[18] The fraction of 35 wt% oxidizing at ~506 °C may be a distribution of heterogeneous SWNT structures (in length and structural quality). The fraction at ~478 °C (23 wt%) may be composed by very defective and short SWNTs and amorphous carbon that still remain.[20] The decomposition at ~650 °C in Figures 1(b) and (c) refers to the oxidation of graphitic nanoparticles.[23]

3.2. Raman Spectroscopy

The results obtained from Raman scattering focus on the evolution of SWNT skeletal disorder obtained via the chemical purification protocol were used in the present work. During strong oxidizing chemical process, it appears possible to create additional defects where carbon atoms are eliminated, the ring structure is open, localized C=C bonds are created, and O-containing groups like carboxyl can be added to the defects to stabilize the structure.[10] Raman scattering has been used for many years as a probe of disorder in the carbon skeleton of sp^2 and sp^3 carbon materials and now this technique has been widely used for characterizing disorder in the nanotube wall.[17, 24] Disorder in the graphene structure of the tube wall is expected to:[17]

(1) decrease the intensity of the Raman-active radial breathing modes (R-band) in the low-frequency spectral region;

(2) increase the integrated intensity and width of the D-band around 1350 cm^{-1}; and

(3) broaden the structure in the G-band near 1590 cm^{-1} appearing besides a shoulder near 1620 cm^{-1} called as G*-band.[2, 17]

Raman spectra (514.5 nm excitation) of SWNT as-grown and processed by the sequential purification protocols discussed previously are shown in Figure 2. The spectra appear in two panels: 100–300 and 1230–1750 cm^{-1}. The intensity of all the spectra was normalized to yield the same intensity for the G-band at ~1590 cm^{-1}. The Raman spectra, from top to bottom in the figure, refer to as-grown (a), after H_2O_2 reflux (b), after HNO_3 reflux (c). The Raman-active radial breathing modes (R-band) are observed at low frequency in the left-hand panel of Figure 2. R-band may have contributions from several tubes simultaneously in resonance with the laser photon frequency. Each component in the R-band has a frequency approximately given by $\omega_{RBM} = 248\ cm^{-1}(nm)/dt\ (nm)$[25] where dt is the tube diameter. In the as-grown CarboLex arc material, the main peak in the R-band is located at ~168 cm^{-1}. This corresponds to a tube diameter of ~1.5 nm.

In the right-hand panel of Figure 2, D- and G-band can be observed. D-band is a relatively broad, disorder-induced band, common in disordered sp^2 carbon materials.[17, 26]

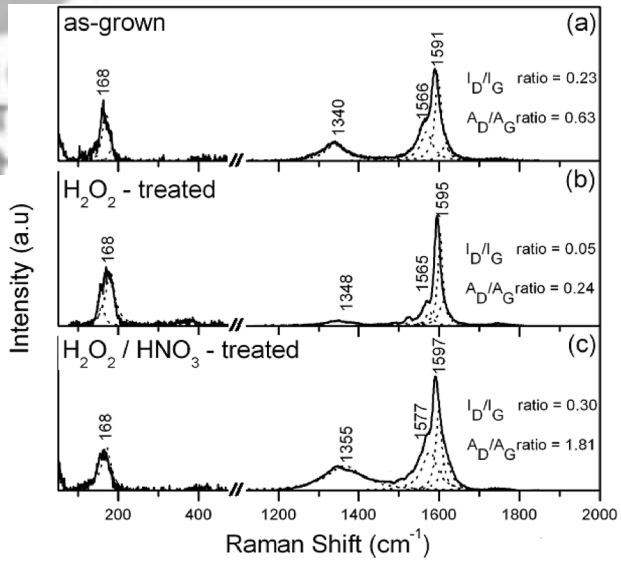

Fig. 2. Raman spectra (laser excitation of 514.5 nm) of the as-grown SWNT (a) and chemically processed SWNT materials: H_2O_2 treated (b) and H_2O_2/HNO_3 treated (c). The spectra appear in two panels: 50–500 cm^{-1} (R-band, left panel) and 1200–2000 cm^{-1} (D- and G-bands, right panel). The dot lines correspond to the Lorentzian fit of the Raman bands. The values I_D/I_G and A_D/A_G (respectively, intensity and area of the D-band relative to the G-band) are indicated in the figure.

G-band for carbon nanotubes is similar to that observed for well-ordered graphite (i.e., E_{2g} band at 1582 cm^{-1}).[17] We have fit the G-bands to a sum of three Lorentzian components and the D-band to only one Lorentzian component. As discussed above, the components can be broadened by disorder in the SWNT skeletal structure. To take advantage of this link between Raman line width and order in the carbon skeleton of the SWNT, we have had to carry out a careful line shape analysis. The D-band is present in all known forms of disordered sp^2 carbons and has been identified with C-atom vacancies during growth or in post-growth purification, substitutional impurities (boron), finite grain or particle effects, or any other symmetry-breaking phenomena.[17, 24] For example, a contribution to the D-band in the as-grown spectrum (Fig. 2(a)) might come from minority phases of disordered sp^2 carbon resulted from the growth process. After oxidation with H_2O_2 to remove the amorphous carbon (Fig. 2(b)), the relative intensity of the D-band is observed to decrease. However, after the nitric acid treatment (second step of the purification process), the relative integrated intensity of the D-band intensity increases, and the D-band broadens and upshifts (Fig. 2(c)). Because the TG data suggest that most of the amorphous carbon has been removed from this sample (Fig. 1(c)), we interpret the increase of the D-band intensity and width after nitric acid refluxing as evidence for a decrease in structural order in the SWNT bundles. Maybe a good way to evaluate the SWNT skeletal disorder is considering the intensity or area of the D-band relative to the G-band. As shown in Figure 2, I_D/I_G and A_D/A_G were found to be high for the as-grown sample, low for the H_2O_2-treated sample and high again for the H_2O_2/HNO_3-treated sample. After these two oxidizing treatment, the D- and G-band have, respectively upshifted by ~4 and 4 cm^{-1} in the first case and ~11 and 6 cm^{-1} in the last case. Previous experimental and theoretical works have shown that removing electrons from SWNT (i.e., p-doping or oxidizing) results in an upshift in the G-band peak,[27] as observed here. This conclusion is consistent with extensive observations of chemical charge transfer reactions in graphite,[28] C_{60},[29] and SWNTs.[27] The upshift of the G-band after refluxing SWNT samples in H_2O_2 and HNO_3 has been identified with electron transfer from the nanotube bundle to form OH^- (Ref. [10]) and NO^{3-} (Refs. [8, 9, 30]) anions, respectively. This interpretation is consistent with work in graphite intercalation compounds.[31] The upshift of the D-band at the same time the G-band is upshifting could be just another signal of charge transfer.

3.3. Infrared Spectroscopy

Infrared (IR) transmission through thin films of the nanotube samples has been used to resolve the structure due to functional groups present in the starting material or added through each step of the chemical process (purification and decarboxilation). IR spectroscopy has been used by several authors to study the SWNT wall chemistry,[11, 13, 30, 32–34] where various functional groups added to the tube wall (e.g., –COOH, –OH, other oxygen containing groups[11, 30, 32–34] and –CH[13]) were identified. However, this task is not trivial, since the percentage of functional groups in the carbon nanotube material is usually very low (~5 wt% at most); only numerous and strongly IR-active groups are detected; and, there is frequently superposition of vibrational modes of the groups present in the complex surface of a chemically processed nanotube sample.

Figure 3 shows the evolution of the mid-IR spectrum of SWNT material before and after chemical process. We can divide the spectra in two regions: 750–2000 cm^{-1} and 2500–4000 cm^{-1}. Between those regions no significant contribution was observed. The spectrum for the as-grown SWNT sample appears at the top. In the high-frequency region of this spectrum, we could only observe a triplet at ~2900 cm^{-1}. Absorption bands occurring around 3000 cm^{-1} are a signature of C–H stretching modes and they are characteristic of the hybridization of the carbon holding the hydrogen atoms. This triplet at ~2900 cm^{-1} is characteristic of sp^3 hybridization and the bands are attributed to symmetrical and asymmetrical C–H stretching vibrations in CH_2 groups and asymmetrical stretching vibrations in CH_3 groups.[35] We could also observe bands at 1397 cm^{-1} ($\upsilon_s CH_3$) and ~1458 cm^{-1} ($\upsilon_{as} CH_3$, $\upsilon_s CH_2$), which could be assigned to C–H bending vibration. Aromatic or vinylic C–H stretching bands occurring between 3000 and 3100 cm^{-1} were not observed. For the as-grown sample, CH_3 or CH_2 groups could not be necessarily attached to the SWNT defects or edges, but

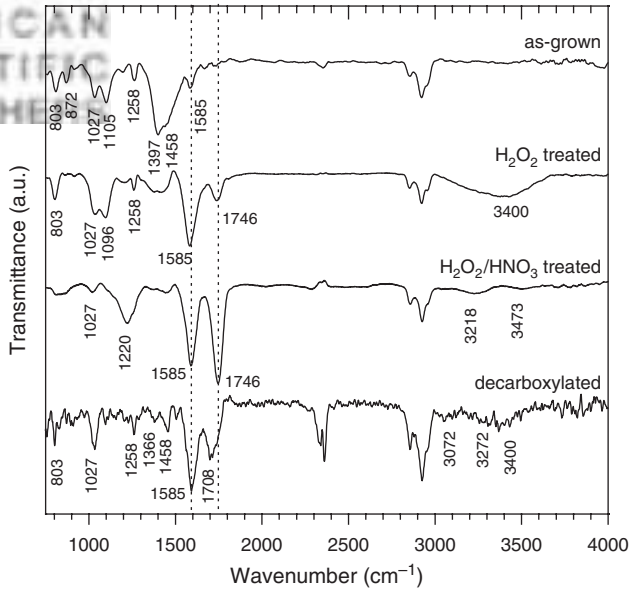

Fig. 3. Micro-FTIR spectra (750–4000 cm^{-1}) with baseline correction of various SWNT films. From top to bottom, the spectra refer to as-grown, H_2O_2-treated, H_2O_2/HNO_3-treated, and decarboxylated SWNT samples.

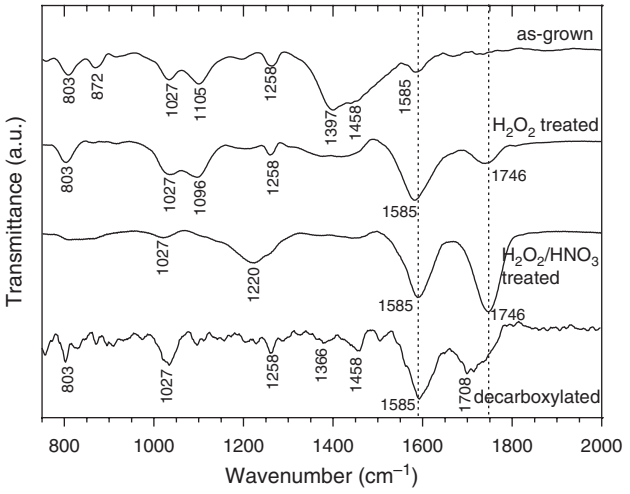

Fig. 4. An expanded scale showing details of the 750–2000 cm^{-1} spectral range of the Micro-FTIR spectra with baseline correction of various SWNT films. From top to bottom, the spectra refer to as-grown, H_2O_2-treated, H_2O_2/HNO_3-treated, and decarboxylated SWNT samples.

instead of that they could be in the amorphous carbon fraction, which come from hydrocarbons adsorbed on the carbon surfaces[36] or even be present in the spectrometer optics. In the low-frequency region, the 1st order SWNT modes appeared at ~803, 872, 1258, and 1585 cm^{-1} (Ref. [10]), and only a modest evidence of oxygen-containing groups was observed. C–O stretching modes of probably ether groups were noticed at ~1027 and 1105 cm^{-1} (Ref. [35]). The spectral range between 750 and 2000 cm^{-1} can be seen with more details in Figure 4.

After H_2O_2 reflux, we can clearly see the appearance of oxygen-containing functional groups. Very broad bands appear in the ~3100–3600 cm^{-1} range and are associated to O–H stretching modes of coupled carboxylic acid and alcoholic or phenolic groups.[10] The width indicates that several different –OH containing groups are probably present in many different chemical and carbon environments. The little band at 1746 cm^{-1} suggest the formation of carboxylic groups (C═O) and the bands at ~1027 and 1096 cm^{-1} could be assigned to C–C–O stretching in unsaturated hydroxyl groups and C–O stretching in ether groups[35]. The band at ~1585 cm^{-1} is assigned to C═C double bonds (1st order E_1 SWNT mode).[10] The removal of amorphous carbon from the SWNT bundle surface and higher exposition of the tube wall could be responsible for increasing the relative intensity of the E_1 mode. The 1st order SWNT modes at 803 and 1258 cm^{-1} were also observed.[10]

Next, we turn to the analysis of the IR spectroscopic signatures that evolve from a sequential H_2O_2/HNO_3 process (Figs. 3(c) and 4(c)). After the acid digestion of the H_2O_2-treated SWNT sample, the main changes in the IR spectrum were:

(1) the very significant enhancement of the absorption associated with the C═O stretching mode of carboxylic groups at 1746 cm^{-1};

(2) the better definition of the bands above 3100 cm^{-1} and

(3) the appearance of a band at ~1220 cm^{-1}.

Even though the intensity of the IR modes in this region has considerably decreased, two distinct bands at ~3218 and 3473 cm^{-1} were identified. These bands are attributed to O–H stretching from carboxylic acid groups and alcoholic or phenolic groups, respectively. The changes suggest a new chemical environment on the SWNT surface. From TG analysis, we know that the SWNT sample is clean from other carbon impurities or adsorbed materials after acid digestion (Fig. 1(c)). So, the picture is consistent with the fact that the oxygen-containing groups are somehow more decoupled and with the formation of additional carboxyl groups on the SWNT surface.[30, 33, 34] The band appearing at ~1220 cm^{-1} probably should be assigned to the C–O bending mode of carboxylic acid and phenolic groups.[35] The only intrinsic SWNT IR-active mode clearly observed was the 1st order E_1 mode at ~1585 cm^{-1}. Shoulders at ~803 and 1258 cm^{-1} could be associated with 1st order SWNT modes.[10]

Finally, we consider the IR signatures after SWNT decarboxylation process. This spectrum appears at the bottom of Figures 3 and 4. Even though the IR spectrum in Figure 3(d) shows some noise, small absorptions near ~3272 and ~1746 cm^{-1}, which could be associated with the presence of some carboxylic group that still remain, were observed. However, three significant changes attest that the decarboxylation reaction has occurred in a good extension. The maximum intensity of the C═O vibrational mode is now at ~1708 cm^{-1}, characterizing the presence of preferentially quinone groups.[35] The C–O bending mode of acid groups (carboxylic acid and phenolic) at ~1220 cm^{-1} has been removed. Moreover, the relative intensity of the C–H stretching mode (relative to E_1 mode around 1585 cm^{-1}) increased considerably. We have measured the band intensity before and after the decarboxylation process by measuring the area under the band after the spectra are converted to absorbance scale. The relative area under the C–H stretching band after decarboxylation was found to be 3 times the area under the same band before the decarboxylation reaction.[13] We believe that the relative increase in the C–H band intensity is due to the exchange from –COOH to –H groups on the SWNT surface, evidencing the occurrence of the decarboxylation reaction and the formation of C–H SWNT derivatives. The reaction mechanism is discussed later in this paper. Possible absorptions at ~3072 cm^{-1} and at ~1458 and 1366 cm^{-1} could be attributed to C–H stretching mode in aromatic rings and C–H bending modes, respectively.[35] By functionalizing SWNT with H atom irradiation, Khare et al.[13] have also found low-intensity C–H bending bands. These authors were not even able to see the aromatic C–H modes.[13]

In Table I, we summarize the main IR bands observed for functional groups in the as-grown soot and chemically

Table I. IR bands observed in the SWNT films: as-grow and chemically processed SWNT materials (H_2O_2-treated, H_2O_2/HNO_3-treated, and decarboxylated).

Observed band (cm^{-1})	Processed SWNT material	Assignment
~3400	H_2O_2 treated	O–H stretching in alcoholic or phenolic groups
~3218	H_2O_2, HNO_3 treated	O–H stretching in coupled carboxylic acid groups
~1746	H_2O_2, HNO_3 treated	C═O stretching in carboxylic acid groups
~1708	Decarboxylated	C═O stretching in quinone groups
~1585	All	1st order SWNT mode
~1285	All	1st order SWNT mode
~1220	H_2O_2, HNO_3 treated	C–O stretching in carboxylic acid and phenolic groups
~1105 and 1027	All	C–C–O stretching in insaturated ethers, esters and alcohols
~872	As-grown	1st order SWNT mode
~803	All	1st order SWNT mode

processed SWNT material, as well as our assignment for those bands. The assignments we make in Table I are plausible but are by no means certain. Follow-up work on model compounds will need to be done to confirm these tentative assignments.

3.4. X-ray Photoelectron Spectroscopy

XPS can give information about the atomic composition of a material surface and the present elements and its coordination number, with sensibility to probe even slight changes in the chemical environment of the carbon nanotube surface. The most widely used data reported in the literature refers to the structure modification of the CNT walls due to the chemical interaction with organic compounds or gases adsorption.[37]

Here, we used XPS to check the changes in the surface chemistry of the SWNT that resulted from the purification and decarboxylation processes. Figure 5 shows the XPS spectral changes among the C1s peaks for as-grown (a), H_2O_2/HNO_3-treated (b) and decarboxylated (c) SWNT samples. The spectra were fit using a combination of Gaussian and Lorentzian curves. The peak position (binding energy) and relative percentages (area under curve) of each chemical bond identified in the SWNT surfaces are displayed in Table II. The as-grown SWNT showed a peak of typical graphitic carbon at 284.5 eV. The slight downshift from the usual C1s energy observed for graphite (284.6 eV) has been explained by the weaker C–C bonds resulting from the curvature of the graphene sheets.[38] Suzuki et al.[39] have demonstrated by using spatially resolved XPS that the shift of the C1*s* binding energy should be only about 50 meV between the tips and the sidewalls of MWNT (multi-wall carbon nanotubes). The strong influence of structural defects on the

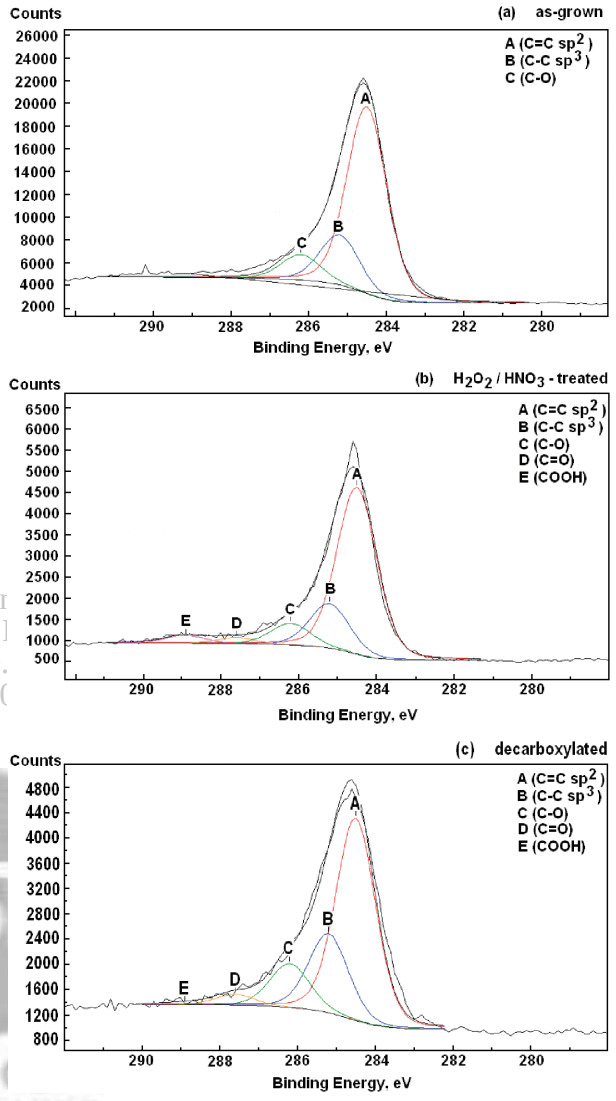

Fig. 5. XPS spectra of the C1s binding energy region with Gaussian-Lorentzian curve fittings for as-grown SWNT (a) and chemically processed SWNT materials: H_2O_2/HNO_3-treated (b), and decarboxylated (c).

electronic structure of MWNT should be responsible for some difference. In fact, Lee et al.[40] have reported that the C1*s* of undoped SWNT are composed of three peaks: sp^2 carbon (peak at about 284.3 eV), sp^3 carbon (285 eV) and oxygen related groups (carboxyl) at about 288.5 eV.

Table II. Relative percentages of the different C–C and C–O bonds obtained from XPS curve fitting of the C1s peaks for as-grown and chemically processed SWNT samples: H_2O_2/HNO_3-treated and decarboxylated.

Bond	Binding energy (eV)	As-grown (%)	H_2O_2/HNO_3 treated (%)	Decarboxylated (%)
C═C sp^2	284.5	71.3	67.7	66.5
C═C sp^3	285.2	19	18.1	20
C—O	286.2	9.7	8.7	10
C═O	287.6	0	2.4	3.2
COOH	288.9	0	3.1	0.3

In our results, we could distinguish two more peaks for the as-grown sample besides the graphitic carbon: one peak at ~285.2 eV assigned to sp^3 carbon and another peak at ~286.2 eV associated with the presence of C–O bonds.[41, 42] Since there is amorphous carbon and possible polyaromatic hydrocarbons in the as-grown SWNT, the peaks assigned to the C1s of sp^3 and oxidized carbon could be elsewhere in the sample.

The purification treatments changed the C1s peak considerably at high binding energies. After an oxidizing procedure using strong oxidant agents like H_2O_2 and HNO_3, it was expected a decrease of the sp^2/sp^3 character ratio in the SWNT C–C bonds and an increase of the numbers of O atoms bonded to C atoms.[43] These changes were observed in Figure 5(b). The shoulder of the main peak became large and it was possible to fit it with a sum of 5 Gaussian-Lorentzian components. The two additional peaks at 287.6 and 288.9 eV were assigned to the C═O and COO groups, respectively.[41, 42]

After the decarboxylation procedure, the main difference of the XPS spectrum (Fig. 5(c)) was a decrease of ~90% in the relative amount of the carboxylic groups present in the purified sample (Fig. 5(b)). Table II shows the values. The removal of carboxylic groups occurred without a significant decrease of the sp^2/sp^3 carbon atom ratio, as observed by Nikitin et al. in their hydrogenation process.[44] Here, the replacement reaction of C–COOH bonds with C–H bonds in the SWNT ends and defects do not seem to have the disadvantage of concomitant loss of the carbon nanotube conjugated electronic structure.

3.5. Acid-Base Potentiometric Tritation

Potentiometric titration is frequently the method of choice for studying the acid-base properties of solid surfaces.[45] The potentiometric titration curves contain information of types, quantity and acid-base strength of the functional surface groups. In the potentiometric titration method the deprotonated groups are detected by the addition of a strong acid that promotes the protonation of the basic sites, being therefore sensitive to low concentrations of acidic sites. Non-linear numerical analysis techniques are commonly used in the treatment of potentiometric data of humic acid, resins, and carbon black.[19, 45–47]

In this work, potentiometric titration in aqueous media and data numerical analysis by non-linear regression techniques, described before for studying the surface of activated carbon,[19] has been applied to distinguish acid groups with different acid strength on the chemically processed SWNT surface. The method allow the determination of the concentration and pKa value of each type of acid group present on the SWNT surface.

The potentiometric titration curves and the nonlinear regression method fitting for the same set of samples as discussed previously are shown in Figure 6. The acidic surface of carbon materials is usually related to the presence

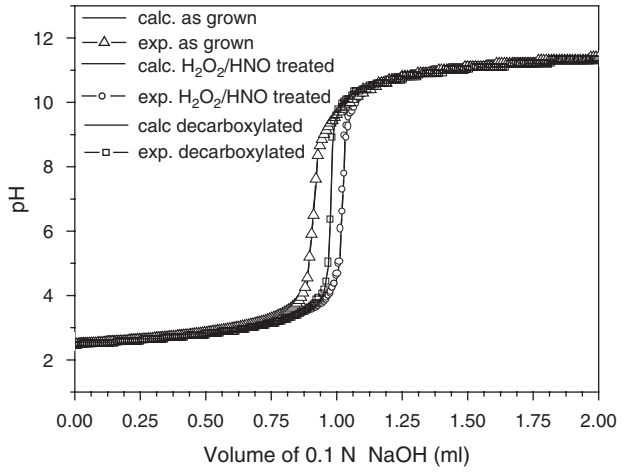

Fig. 6. Potentiometric titration curves, in 0.01 mol · liter^{-1} KCl for as-grown SWNT (a) and chemically processed SWNT materials: H_2O_2/HNO_3-treated (b), and decarboxylated (c). The symbols refer to the experimental data. The solid lines represent the curves obtained by nonlinear regression program used in this work.[19]

of anhydrides, carboxylic, lactonic, and phenolic groups. The oxidation by nitric acid (the second step of our purification protocol) is known to be an effective means to provide acid carboxylic and phenolic groups on SWNT surface,[10] as discussed before in this paper. However, due to the complex chemical environment of the SWNT surface, the carboxylic group introduced on that surface can exhibit a spread of their dissociation constant, depending on the neighboring groups.[48] So, the curves in Figure 6 were fit considering the pKa values in the range of phenolic and carboxylic groups and IR spectroscopy and XPS analyses. The results are summarized in Table III. Basically, two different acid functions were distinguished in our SWNT samples. The groups related to pKa between 2.0 and 6.0 were associated with carboxylic acids and those related to pKa between 9.0 and 12.5 were identified with phenolic functions. The numbers in Table III show that both purification and decarboxylation process change the chemical environment on the SWNT surface. The sequential H_2O_2 and HNO_3 treatments introduce considerably acid groups at both pKa ranges. On the other hand, the decarboxylation process decreases the number of carboxylic acid groups in about 97%. These results confirm the efficiency of the decarboxylation procedure proposed here for SWNT. They also corroborate with the evidence

Table III. Functional group content of as-grown, H_2O_2/HNO_3-treated, and decarboxylated SWNT samples analyzed by potentiometric titration.

	Acid sites (mmol/g)	
Sample	pKa 2.0–6.0	pKa 9.0–12.5
As-grown	0.43	1.81
H_2O_2/HNO_3 treated	10.45 (pKa = 2.6) 1.02 (pKa = 3.5)	9.59
Decarboxylated	0.31 (pKa = 6.0)	5.95

from IR and XPS results of the formation of ketone groups after the decarboxylation reaction. However, the chemistry behind these functional groups additions needs to be clarified in further work.

3.6. The Decarboxylation Process

Based on all results discussed here the decarboxylation procedure using copper(I) oxide and quinoline at high temperatures and under inert atmosphere has shown to rend high yields of C–H SWNT derivatives.

Cohen and Schambach (1970)[15] suggested for the first time a mechanism for the loss of carbon dioxide in copper-quinoline decarboxylation of aromatic structures. They proposed that the copper(I) ion forms a π-complex with the aromatic ring of the carboxylate anion. Loss of carbon dioxide from the complex yields a σ-carbanion stabilized by the π-complexed metal ion. This species then collapses to an arylcopper(I) compound that can react with a source of protons and produce the decarboxylated product. In accord to the authors the presence of oxygen decreases the concentration of cuprous ion and increases that of cupric ion, which causes an oxidative decarboxylation.

The study of products, kinetics, mechanism and the use of quinoline and pyridine as solvent were explored later by Cohen et al.[16] By using gas–liquid chromatography (GLC), they identified quali and quantitatively the products of the decarboxylation derived from the cuprous carboxylate (carbon dioxide and arene) and those derived from the quinoline (aryl and acylquinolines, biquinolyls, and oxybiquinolyls). The by-products derived from the quinoline were formed because the quinoline acts in the reactional medium not only as a solvent, but also as the major source of protons to produce the arene. The protons seem to be slowly generated during the various coupling reactions of the quinoline.

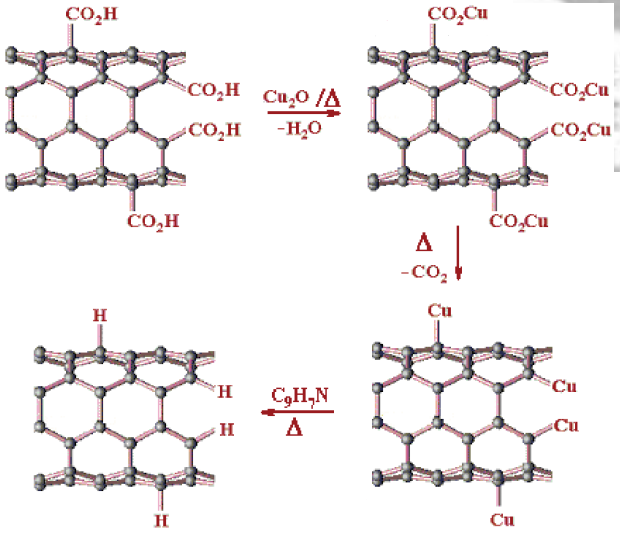

Fig. 7. A schematic representation for the decarboxylation reaction of oxidized SWNT. Oxidized SWNT containing mainly carboxylic acid groups were treated with copper(I) oxide in a mixture of quinoline and N-methylpyrrolidinone at high temperature under argon inert atmosphere. The heating of cuprous oxide with carboxylic acids form cuprous carboxylate and water. The cuprous carboxylate loss carbon dioxide to rend an arylcopper(I) compound which react with a source of protons (quinoline) and produce the decarboxylated product.

In 1997 Stock and Obeng investigated several reagents for the decarboxylation of naphthalene-2-carboxylic acid and the results led to the use copper (I) oxide in a mixture of *N*-methylpyrrolidinone and quinoline (50:50).[49] This mixture were successfully used for the decarboxylation of oxidized coal by Stock and Obeng and oxidized SWNT at the present work.

We show in Figure 7 a schematic representation for the decarboxylation reaction of oxidized SWNT. The by-products are not represented. The open end caps of SWNT decorated with carboxyl groups illustrate the aromatic carboxylic acid sites which suffered the decarboxylation process.

4. CONCLUSIONS

In summary, we have succeeded in performing the decarboxylation of oxidized SWNT rendering C–H SWNT derivatives. The interesting finding of this study is to observe that a classical protocol amply used in organic chemistry of aromatic and polyaromatic molecules works for the complex environment on the SWNT surface. The reaction was performed using copper(I) oxide in a 50:50 solution of *N*-methylpyrrolidone and quinoline. FTIR, XPS, and acid-base potentiometric titration analyses were carried out to characterize quali and quantitatively the changes in the chemical environment on the SWNT surface in each step of the purification and decarboxilation process. Those techniques showed the appearance of mainly carboxylic and phenolic groups after the sequential H_2O_2 and HNO_3 refluxes and the disappearance of the carboxylic groups after the decarboxylation reaction. FTIR analysis indicated also the formation of aliphatic and aromatic C–H groups. XPS and potentiometric titration results determined an efficiency higher than 90% for our decarboxylation procedure. The purity and structural quality of the single-wall carbon nanotubes used in the decarboxylation process were evaluated by TG and Raman spectroscopy. TG analysis identified a purified sample with ~80 wt% of SWNT, in fractions distributed in highly structured SWNTs (25 wt%), with distribution in composition, length and structural quality (35 wt%) and with very defective and short tubes (25 wt%). The damages on the purified SWNT walls were characterized by the Raman scattering analysis.

Acknowledgments: The authors acknowledge Prof. Peter Eklund, from The Pennsylvania State University, for providing us the SWNT samples. We also thank Alexandre S. dos Santos and Carlos R. Gonçalves for help with TG

measurements. Work supported by the Brazilian Network on Carbon Nanotube Research and Millennium Institute of Nanotechnology, CNPq, CNEN, and FAPEMIG (Brazil).

References and Notes

1. M. S. Dresselhaus, G. Dresselhaus, and P. C. Eklund, Science of Fullerenes and Carbon Nanotubes, Academic, San Diego (**1996**).
2. M. S. Dresselhaus, G. Dresselhaus, and P. Avouris, Carbon Nanotubes: Synthesis, Properties and Applications, Springer-Verlag, Berlin (**2001**).
3. S. Niyogi, M. A. Hamon, H. Hu, B. Zhao, P. Bhowmik, R. Sen, M. E. Itkis, and R. C. Haddon, *Acc. Chem. Res.* 35, 1105 (**2002**).
4. S. Banerjee, T. Hemraj-Benny, and S. S. Wong, *Adv. Mater.* 1, 17 (**2005**).
5. A. G. Rinzler, J. Liu, H. Dai, P. Nikolaev, C. B. Huffman, F. J. Rodriguez-Macias, P. J. Boul, A. H. Lu, D. Heymann, D. T. Colbert, R. S. Lee, J. E. Fischer, A. M. Rao, P. C. Eklund, and R. E. Smalley, *Appl. Phys. A* 67/1, 29 (**1998**).
6. I. W. Chiang, B. E. Brinson, A. Y. Huang, P. A. Willis, M. J. Bronikowski, J. L. Margrave, R. E. Smalley, and R. H. Hauge, *J. Phys. Chem. B* 105/35, 8297 (**2001**).
7. A. R. Harutyunyan, B .K. Pradhan, J. P. Chang, G. Chen, and P. C. Eklund, *J. Phys. Chem. B* 106, 8671 (**2002**).
8. C. A. Furtado, U. J. Kim, H. R. Gutierrez, L. Pan, E. C. Dickey, and P. C. Eklund, *J. Am. Chem. Soc.* 126/19, 6095 (**2004**).
9. O. Zhou, B. Gao, C. Bower, L. Fleming, and H. Shimoda, *Mol. Cryst. Liq. Cryst. Sci. Technol. Sect. A* 340, 541 (**2000**).
10. U. J. Kim, C. A. Furtado, X. Liu, G. Chen, and P. C. Eklund, *J. Am. Chem. Soc.* 127/44, 15437 (**2005**).
11. D. B. Mawhinney, V. Naumenko, A. Kuznetsova, J. T. Yates, J. Liu, and R. E. Smalley, *J. Am. Chem. Soc.* 122/10, 2383 (**2000**).
12. T. Dimitrios, T. Nikos, G. Vasilios, and P. Maurizio, *Chem. Eur. J.* 9/17, 4000 (**2003**).
13. B. N. Khare, M. Meyyappan, A. M. Cassell, C. V. Nguyen, and J. Han, *Nano Lett.* 2/1, 73 (**2002**).
14. A. F. SheDard, N. R. Winslow, and J. R. Johnson, *J. Am. Chem. Soc.* 52, 2083 (**1930**).
15. T. Cohen and R. A. Schambach, *J. Am. Chem. Soc.* 92, 3189 (**1970**).
16. T. Cohen, R. W. Berninger, and J. T. Wood, *J. Org. Chem.* 43, 837 (**1978**).
17. M. S. Dresselhaus, G. Dresselhaus, M. A. Pimenta, and P. C. Eklund, Analytical Applications of Raman Spectroscopy, edited by M. J. Pelletier, Blackwell Science, Cambridge, MA (**1999**), Chap. 9.
18. M. A. Pimenta, A. Marucci, S. Empedocles, M. Bawendi, E. B. Hanlon, A. M. Rao, P. C. Eklund, R. E. Smalley, G. Dresselhaus, and M. S. Dresselhaus, *Phys. Rev. B* 58, R16016 (**1998**).
19. J. P. Mesquita, P. B. Martelli, and H. F. Gorgulho, *J. Braz. Chem. Soc.* 17, 1133 (**2006**).
20. Z. Shi, Y. Lian, F. Liao, X. Zhou, Z. Gu, Y. Zhang, and S. Iijima, *Solid State Commun.* 112, 35 (**1999**).
21. B. J. Landi, C. D. Cress, C. M. Evans, and R. P. Raffaelle, *Chem. Mater.* 17, 6819 (**2005**).
22. H. Hui, B. Zhao, M. E. Itkis, and R. C. Haddon, *J. Phys. Chem. B* 107, 13838 (**2003**).
23. P. M. Ajayan, T. W. Ebbesen, T. Ichihashi, S. Iijima, K. Tanigaki, and H. Hiura, *Nature* 362, 522 (**1993**).
24. M. A. Pimenta, A. Jorio, S. D. M. Brown, A. G. S. Filho, G. Dresselhaus, J. H. Hafner, C. M. Lieber, R. Saito, M. S. Dresselhaus, and M. Endo, *Phys. Rev. B* 59, R6585 (**1999**).
25. A. Jorio, R. Saito, J. H. Hafner, C. M. Lieber, M. Hunter, T. McClure, G. Dresselhaus, and M. S. Dresselhaus, *Phys. Rev. Lett.* 86/6, 1118 (**2001**).
26. Y. Wang, D. C. Alsmeyer, and R. L. McCreery, *Chem. Mater.* 2, 557 (**1990**).
27. A. M. Rao, P. C. Eklund, S. Bandow, A. Thess, and R. E. Smalley, *Nature* 388, 257 (**1997**).
28. P. C. Eklund and K. R. Subbaswamy, *Phys. Rev. B* 20, 5157 (**1992**).
29. P. Zhou, K. A. Wang, Y. Wang, P. C. Eklund, M. S. Dresselhaus, G. Dresselhaus, and R. A. Jishi, *Phys. Rev. B* 46, 2595 (**1992**).
30. A. Kukovecz, C. Kramberger, M. Holzinger, H. Kuzmany, J. Schalko, M. Mannsberger, and A. J. Hirsch, *Phys. Chem. B* 106/25, 6374 (**2002**).
31. G. U. Sumanasekera, J. L. Allen, S. L. Fang, A. L. Loper, A. M. Rao, and P. C. Eklund, *J. Phys. Chem. B* 103, 4292 (**1999**).
32. M. T. Martinez, M. A. Callejas, A. M. Benito, M. Cochet, T. Seeger, A. Anson, J. Schreiber, J. C. Grodon, C. Marhic, O. Chauvet, J. L. G. Fierro, and W. K. Maser, *Carbon* 41, 2247 (**2003**).
33. J. Zhang, H. Zou, Q. Qing, Y. Yang, Q. Q. Li, Z. Liu, X. Gao, and Z. Du, *J. Phys. Chem. B* 107/16, 3712 (**2003**).
34. M. A. Hamon, H. Bhowmik, P. Hu, S. Niyogi, B. Zhao, M. E. Itkis, and R. C. Haddon, *Chem. Phys. Lett.* 347, 8 (**2001**).
35. R. M. Silverstein and F. X. Webster, Spectrometric Identification of Organic Compounds, John Wiley & Sons, New York (**1998**), Chap. 3.
36. S. E. Weber, S. Talapatra, C. Journet, A. Zambano, and A. D. Migone, *Phys. Rev. B* 61, 13150 (**2000**).
37. T. Belin and T. F. Epron, *Mater. Sci. Eng. B* 119, 105 (**2005**).
38. P. Chen, X. Wu, X. Sun, J. Lin, W. Ji, and K. Tan, *Phys. Rev. Lett.* 82, 2548 (**1999**).
39. S. Suzuki, Y. Watanabe, T. Ogino, S. Heun, L. Gregoratti, A. Barinov, B. Kaulich, M. Kiskinova, W. Zhu, C. Bower, and O. Zhou, *Phys. Rev. B* 66, 035414 (**2002**).
40. Y. Lee, T. Cho, B. Lee, J. Rho, K. An, and Y. Lee, *J. Fluorine Chem.* 120, 99 (**2003**).
41. T. I. T. Okpalugo, P. Papakonstantinou, H. Murphy, J. McLaughlin, N. M. D. Brown, and T. McNally, *Fullerenes, Nanotubes, and Carbon Nanostructures* 13, 477 (**2005**).
42. K. H. An, J. S. Park, Cheol-Min Yang, S. Y. Jeong, S. Chu Lim, Chul Kang, Joo-Hiuk Son, M. S. Jeong, and Y. H. Lee, *J. Am. Chem. Soc.* 127/14, 5196 (**2005**).
43. S. Banerjee and S. S. Wong, *J. Phys. Chem. B* 106, 12144 (**2002**).
44. A. Nikitin, H. Ogasawara, D. Mann, R. Denecke, Z. Zhng, H. Dai, K. Cho, and A. Nilsoon, *Phys. Rev. Lett.* 95, 225507 (**2005**).
45. J. C. Masini, *Anal. Chim. Acta* 283, 803 (**1993**).
46. V. S. Soldatov, Z. I. Sosinovich, T. A. Korshunova, and T. V. Mironova, *React. Funct. Polym.* 58, 3 (**2004**).
47. A. Contescu, C. Contescu, K. Putyera, and J. A. Schwarz, *Carbon* 35, 83 (**1997**).
48. J. L. Figueiredo, M. F. R. Pereira, M. M. A. Freitas, and J. J. M Órfão, *Carbon* 37, 1379 (**1999**).
49. L. M. Stock and M. Obeng, *Energy Fuels* 11, 987 (**1997**).

Received: 15 May 2006. Accepted: 22 September 2006.